Electronic Supplementary Material (ESI) for Nanoscale.

Supporting Information

Pseudo single domain colloidal superparamagnetic nanoparticles designed at the physiologically tolerable AC magnetic field for clinically safe hyperthermia

Authors

Ji-wook Kim[1+], Dan Heo[2+], Jie Wang[1], Hyung-sub Kim[1], Satoshi Ota[3], Yasushi Takemura[4], Chulhaeng Huh[2], and Seongtae Bae[*,1]

[1]Nanobiomagnetics and Bioelectronics Laboratory (NB[2]L), Department of Electrical Engineering, University of South Carolina, Columbia, SC 29208, USA

[2]MCG-Radiation Oncology, Georgia Cancer Center, Augusta University, Augusta, GA 30912, USA

[3]Electrical and Electronic Engineering, Shizuoka University, Hamamatsu 432-8561, Japan

[4]Electrical and Computer Engineering, Yokohama National University, Yokohama, 240-8501, Japan

*Corresponding author

E-mail: bae4@cec.sc.edu

[+]These two authors equally contributed to this work.

Section 1. X-ray diffraction patterns of Mg-doped γ-Fe_2O_3 MNPs

The crystal structure was analyzed using a Cu-Kα radiated X-ray diffractometer. All the synthesized Mg-doped γFe_2O_3 MNPs showed a single-phase cubic spinel ferrite structure and did not exhibit any undesirable crystalline phases. All the X-ray diffraction patterns of Mg-doped γFe_2O_3 MNPs were well indexed and correlated to those of typical cubic spinel structures (JCPDS #38-0430)

Section 2. X-ray absorption near edge structure (XANES) analysis

We have performed Fe K-edge XANES analysis for Mg-doped γFe_2O_3 MNPs to determine the local atomic structure. Fe K-edge X-ray absorption spectra were recorded on the BL10C beamline of the Pohang light source II (PLS-II) with a ring current of 360 mA at 3.0 GeV under top-up operation. Si (111) double crystal monochromator has been employed to monochromatize the X-ray photon energy. The incident and transmitted X-ray photon flux were monitored with N2 gas-filled ionization. The EXAFS data from the samples were collected under the transmittance mode. Higher-order harmonic contaminations were eliminated by detuning to reduce the incident X-ray intensity by a ~30 %. Energy calibration has been simultaneously carried out for the measurement with a Fe metallic film placed in front of the third ion chamber. Fourier transform (FT) peak feature of Mg-doped γ-Fe_2O_3 MNPs showed the typical radial distribution function of Mg-doped γ-Fe_2O_3 (maghemite). The decrease in the FT peak intensity (O_h-T_d corner shaped) can be attributed to the evolution of Fe defect site (for example, iron vacancy site) by the occurrence of Fe^{3+} ions.

Section 3. DC magnetization measurement

The DC M-H loops (major and minor loops) were measured using a vibrating sample magnetometer (VSM). Colloidal Mg-doped γFe_2O_3 was used for all measurements to observe magnetization behaviors

of MNP colloids. For the measurement, a 0.08 mL of Mg-doped γFe_2O_3 nanofluid (10 mg/mL) was loaded to the sample holder. Demagnetization field was applied before measurement. DC magnetic field with a sweeping of -5000 ~ 5000 Oe and -150 ~ 150 Oe were applied for major and minor M-H loop measurements, respectively. For FC/ZFC curve measurement, a magnetic property measurement system (MPMS) was utilized. FC/ZFC curve was obtained at 4K ~ 300 K with 10 K interval. Mg-doped γFe_2O_3 MNPs powder was used for FC/ZFC curve measurements.

Section 4. AC magnetic susceptibility measurement

To obtain the out-of-phase susceptibility of Mg-doped γFe_2O_3 MNPs, AC hysteresis was measured using a physical property measurement system (PPMS). Mg-doped γFe_2O_3 nanofluid was used for all measurements to observe the magnetization behaviors of colloidal MNPs. In order to study the AC magnetic hysteresis behavior of Mg-doped γFe_2O_3 MNPs, the AC M-H loops were measured using an AC solenoid coil capacitor system at the fixed H_{appl} of 9.54 kAm^{-1}, and the f_{appl} of 100 kHz, respectively.

Section 5. Blocking temperature and magnetic anisotropy constant measurement

To clarify the magnetic phase of Mg-doped γFe_2O_3 MNPs, the blocking temperature (T_B) was determined by employing the ZFC/FC measurement. As can be seen in Figure 2a, 13 and 25 nm (d_{MNP}) of Mg-doped γFe_2O_3 MNP had a well-defined T_B of 50 K and 280 K, respectively. This result demonstrates that Mg-doped γFe_2O_3 MNP can show superparamagnetic behaviors at room temperature. Calculated anisotropy constant of 13 and 25 nm of Mg-doped γFe_2O_3 MNPs based on the following equation was 1.19×10^4 J/m^3 and 1.21×10^4 J/m^3, respectively. All relaxation time constant values are described in Table S1.

$$T\mathrm{B} = \frac{K_{\mathrm{u}}\mathrm{V}}{k\mathrm{B}\ln(\frac{\tau_m}{\tau_0})}$$

($\tau 0$: a characteristic attempt time, typically taken as around 10^{-9} s, τm: time to make a measurement, typical $\ln(\frac{\tau m}{\tau 0})$ is 25)

Section 6. In-vitro toxicity test

The human prostate cancer cell line, LNCaP (ATCC® CRL-1740™, ACTT, VA, USA), was cultured with RPMI-1640 culture media containing 10% fetal bovine serum. In vitro toxicity tests of PSD-SPNP were carried out using MTT assay. Briefly, 1×10^4 cells/well of LNCaP cells were seeded on 96-well plate and incubated at 37°C and 5% CO_2 with humidified atmosphere for 24 h. PSD-SPNP was prepared in various concentration (0, 50, 100, 200, 500 and 1000 μg/mL) within the culture media. They were added into each well (n=5) and incubated for 24 h and 48 h. After then, all media were removed and each well was washed with Dulbecco's phosphate buffered saline (DPBS, HyClone™ DPBS 1x, GE Healthcare, UK). All wells were filled with 0.1 mL of fresh culture media. Next, 10 μL of MTT reagent (Alfa Aesar™ Thiazolyl Blue tetrazolium bromide, 98%, Thermo Fisher Scientific, MA, USA) was added in each well, which was incubated for 3 h. All media were discarded and 10% SDS solution was added to dissolve the formazan crystals. Finally, the 96-well plate was incubated overnight at 37°C on the orbital shaker for 30min and measured using microplate reader (Benchmark plus, Bio-Rad Laboratories, CA, USA). The optical density value of each well from the microplate reader was normalized by control group's and represented as percentages.

Section 7. Blood chemistry test of PSD-SPNP

All animal experiments were conducted with the approval of the Association for Assessment and Accreditation of Laboratory Animal Care International. All nanofluids were dispersed in DPBS before the experiments. Eight weeks aged C57BL/6 mice were selected for this experiment and divided into 4 groups (0, 0.7, 7, 70 mg/kg of PSD-SPNP, n = 10 of each group). PSD-SPNP were injected into the tail vein of mice. After 7 days, all mice were euthanized and we collected the blood from each mice. The red blood cell (RBC) count was observed using a hematocytometer and alanine aminotransferase (ALT), aspartate transaminase (AST), blood urea nitrogen (BUN), and serum creatinine concentration analysis was carried out after separating the serum from whole blood using each detection kit (ALT, AST, serum creatinine assay kit, Sigma-Aldrich Inc., USA; BUN assay kit, thermo-fisher scientific Inc., USA). Each assay was performed by following the manufacturer's experimental guideline.

Section 8. In-vitro MNFH test

All nanofluids were dispersed in cell culture media before the experiments. LNCaP cells were cultured at a 96-well plate for 24 h (1×10^4). The culture media of LNCaP cells was exchanged with 0, 1, 2, and 5 mg/mL of Feridex, PSD-SPNP, and MP-SPNP. The heating bed was warmed up to 37^{o}C and the cell culture plate was placed on the top of the heating bed. A small hole (~1 mm) was made at the center of cell culture plate cover to put a fiber-optic thermometer for monitoring of the temperature. Then, all components of the heating bed, cell culture plate, and fiber-optic thermometer were placed in the AC magnetic coil and AC magnetic field (f_{appl}: 100 kHz, H_{appl}: 140 Oe) was applied for 25 min. Next, all wells of the plate were washed 3 times with DPBS and incubated for 24 h. After then, we investigated cell viability using MTT assay.

Section 9. In-vivo MNFH Study

All animal experiments were conducted with the approval of the Association for Assessment and Accreditation of Laboratory Animal Care International. The LNCaP xenograft mice were prepared for in-vivo MNFH test. Briefly, 2×10^6 cells of LNCaP were implanted in the right thigh of athymic nude mice (Balb/c nude). When the tumor volume grew more than 0.25 mL, the mice were divided into 5 groups (0, 2.5, 5.0. 7.5 mg/mL$_{tumor}$ of PSD-SPNP and P-SPNP). The nanofluids were injected into the tumor directly using motorized/multi-channel injection. The injection speed was 5 μL/min. The volume of tumore was 0.25 ~ 0.35 mL and the injected volume of MNP was 70 μL (10 μL of MNP was seperatly injected into 7 tumor site as shown as Figure 5a). The MNFH was carried out for 25 min. After MNFH, the tumor volume and body weight of the animals were followed up for 10 days.

Section 10. Simulation of mass transfer and bio-heat transfer

In order to make optimal injection strategy for the in-vivo magnetic hyperthermia study, we described a specific model that was used to evaluate the concentration and temperature distribution in the tumor based on the mathematical modeling and simulation approach. A finite element analysis (FEA) simulation was conducted in COMSOL Multiphysics. The diffusion of PSD-SPNP, heat dissipation and heat transfer of the nanofluid were solved by convection-diffusion model, Rosensweig's theory and Penne's bio-heat equation. To implement the hyperthermia process, we constructed a simplified model consisting of tumor tissue and PSD-SPNP with different concentration was directly injected into the tumor. The tumor shape was considered to be ellipsoid with a-semiaxis of 6.75 mm and b-semiaxis of 5.1mm based on the size of the Xenograft mouse model with 0.3 mL of tumor volume. Initial nanofluid distribution was assumed to be spherical shape since our injection rate is very low (10 μL/min). Injection concentrations of 10, 20, and 30 mg/mL were used for 2.5, 5.0, and 7.5 mg/mL$_{tumor}$, respectively, from our experimental conditions. After injection of the nanofluid into a tumor, the nanofluid forms a cavity near the needle tip and the nanofluid starts to diffuse within the tumor, which we modeled through the convection-diffusion equation:

$\frac{\partial c}{\partial t} = D \cdot \nabla c$, where c is the molar concentration of nanofluid, and D is a diffusion coefficient that can be solved by the Stokes-Einstein equation. Cacluated D of PSD-SPNP is 1.0×10^{-10} m^2/s. Heat generation of MNP under AC magnetic field is given by the R.E. Rosensweig formulation $Q_{mnp} = \mu_0\chi_0 H_0^2 f_0 \chi''$[1,2]. The temperature filed in the biological tissue can be calculated using Penne's bio-heat equation: $\rho_t c_t \frac{\partial T_t}{\partial x} = k_t \nabla^2 T_t + \omega_t \rho_b c_b (T_b - T_t) + Q_{met} + Qnp$[3,4]. All the relevant parameters and the physical properties of the tissues for solving last two equations could be found on references of 2,4-7[2,4–7].

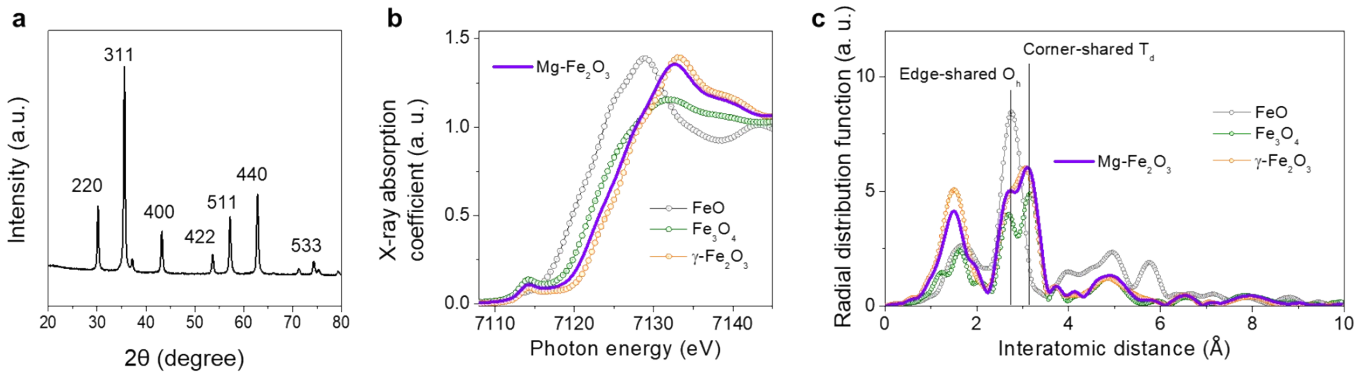

Figure S1. Crystal structure analysis of Mg-doped γFe_2O_3 MNPs. X-ray diffraction pattern (a), Fe K-edge XANES spectra (b), and Fe K-edge radial distribution function (c) of Mg-doped γFe_2O_3 MNPs.

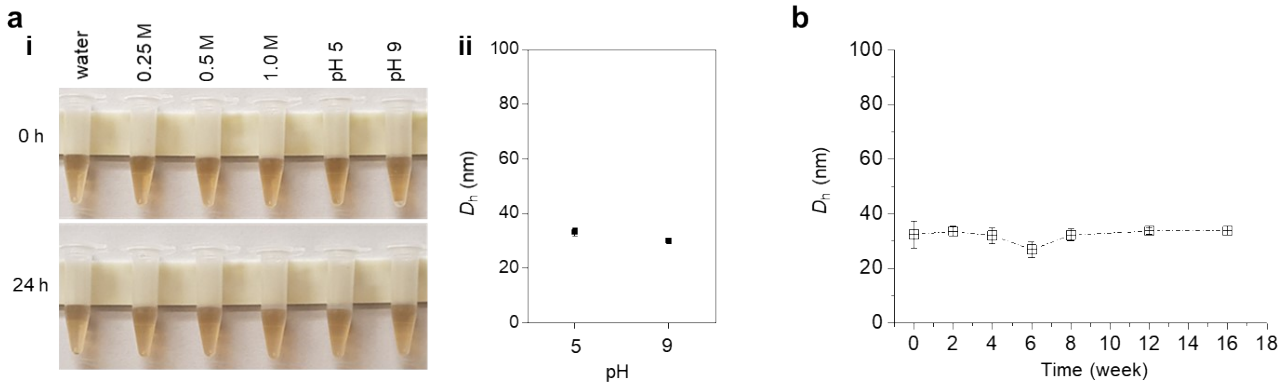

Figure S2. Colloidal stability test of PSD-SPNP. (a) A picture of pH and salt stability test (i) and D_h (ii) of Mg-doped γFe_2O_3 nanofluid. D_h measured in NaCl salt solution is shown in Figure 3a(ii). (b) Long-term stability test of PSD-SPNP. D_h were monitored for 16 weeks. PSD-SPNPs were dispersed in water.

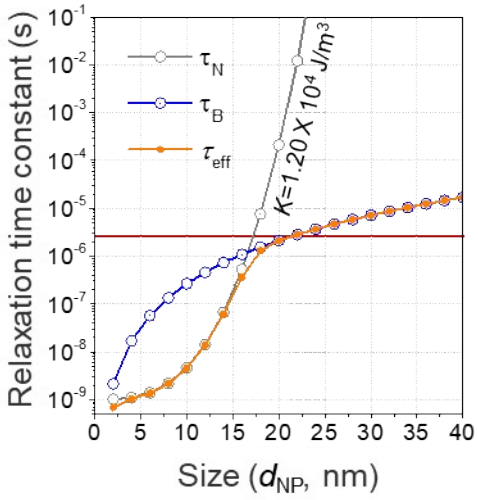

Figure S3. Calculated Nèel (τ_N), Brownian (τ_B), and effective (τ_{eff}) relaxation times of 2 ~ 40 nm Mg-doped γFe_2O_3 MNP from experimentally measured anisotropy constant and hydrodynamic size.

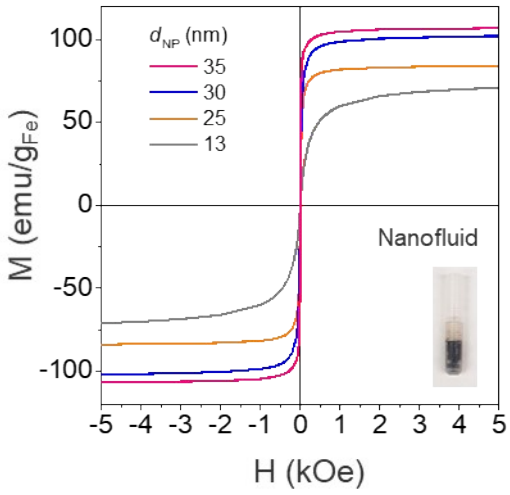

Figure S4. Major M-H loop of 13, 25, 30, and 35 nm (d_{NP}) dextran coated Mg-doped γFe_2O_3 MNP measured at the DC sweeping magnetic field of ±5k Oe.

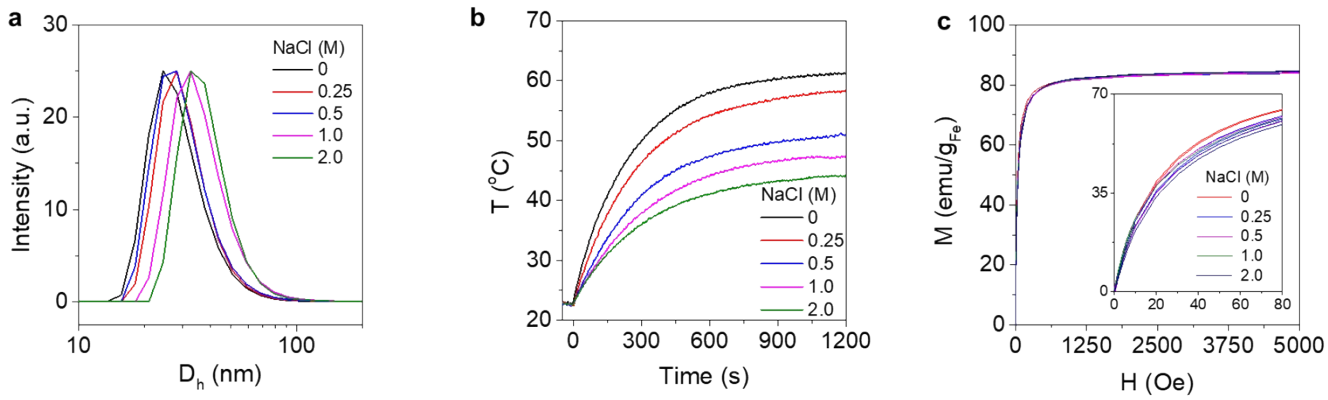

Figure S5. Hydrodynamic size, AC magnetic self-heating temperature rising characteristics, and magnetization analysis of aggregated PSD-SPNP. (a) D_h of PSD-SPNP measured at 0, 0.1, 0.5, 1.0, and 2.0 M of NaCl solution. (b) AC magnetic self-heating temperature rising characteristics of PSD-SPNP dispersed in 0, 0.25, 0.5, 1.0, and 2.0 M NaCl solution. (c) Major M-H loops of PSD-SPNP dispersed in 0, 0.25, 0.5, 1.0, and 2.0 M NaCl solution measured at the DC magnetic field. Inset: minor M-H loop.

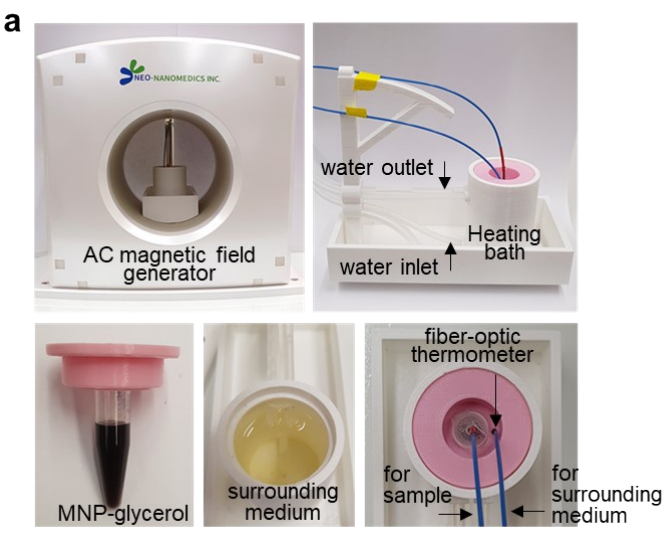

Figure S6. (a) Pictures of experimental setup including AC magnetic field generator, tissue-mimicking glycerol phantom, a heating bath with inlet and outlet for water circulation, and two fiber-optic thermometers for the temperature monitoring of nanofluid and surrounding medium. (b) A temperature monitoring of nanofluid and surrounding medium in tissue-mimicking glycerol phantom during the MNFH. The surrounding medium (green) keeps the temperature at 37°C during the application of AC magnetic field (f_{appl}: 100 kHz, H_{appl}: 120 Oe) while the temperature of PSD-SPNP was increased (orange).

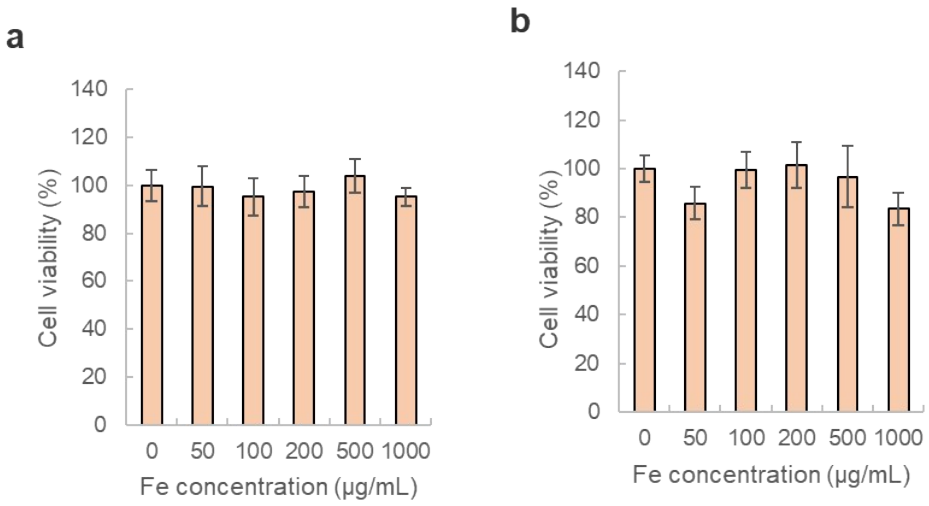

Figure S7. Cell toxicity test of PSD-SPNP. MTT assay was performed after incubation of PSD-SPNP for 24 h (a) and 48 h (b).

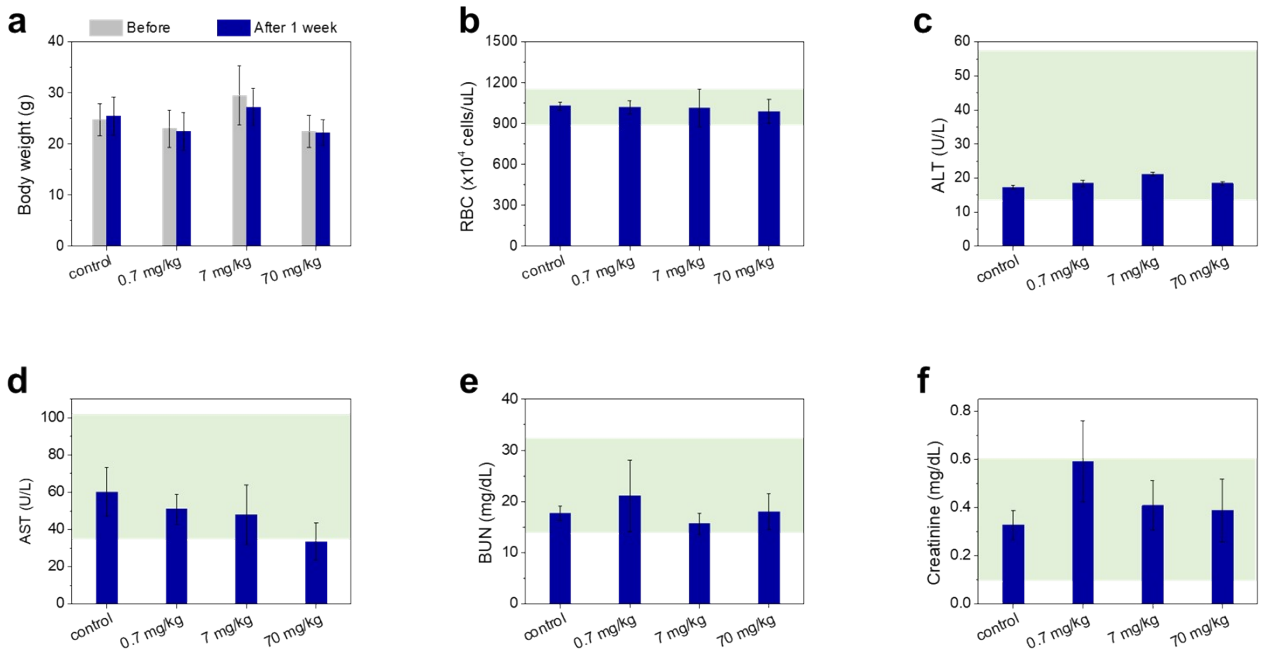

Figure S8. (a) Body-weight changes of mice after intravenous administration of PSD-SPNP. (b-f) Blood chemistry test of PSD-SPNP. Red blood cell (RBC) counting (b), alanine aminotransaminase (ALT) (c), aspartate aminotransaminase (AST) (d), blood urea nitrogen (BUN) (e), and serum creatinine concentration (f) changes after intravenous administration of PSD-SPNP: The body weight was not changed at the 0 ~ 70 mg/kg injection dose. In addition, from the blood chemistry tests of blood counts (red blood cells), liver enzyme levels (Alanine aminotransaminase (ALT) and aspartate aminotransaminase (AST)), and kidney function (blood urea nitrogen (BUN) and creatinine), all results were in the normal range at 1 week after intravascular injection.

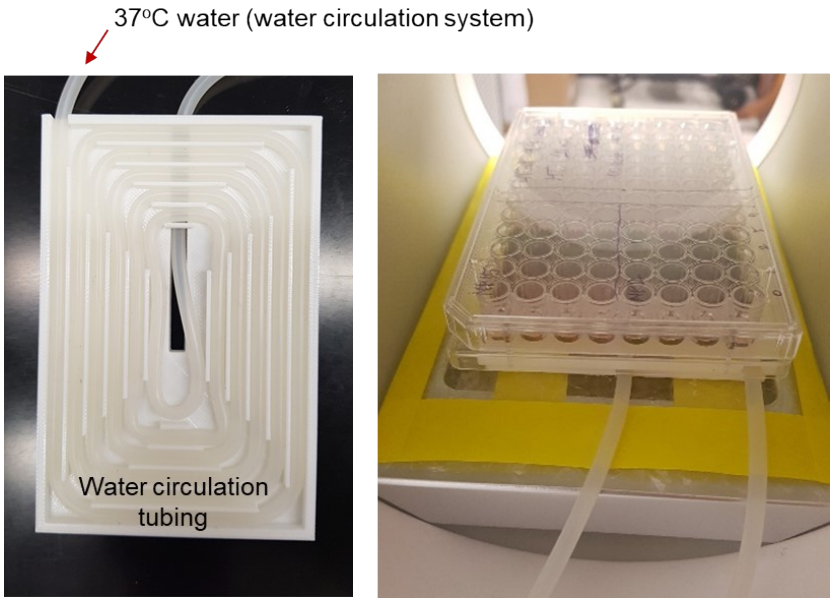

Figure S9. Pictures of heating bed for in vitro cell MNFH test. (left) Inside structure of the heating bed. (right) 96 cell culture plate mounted the heating bed.

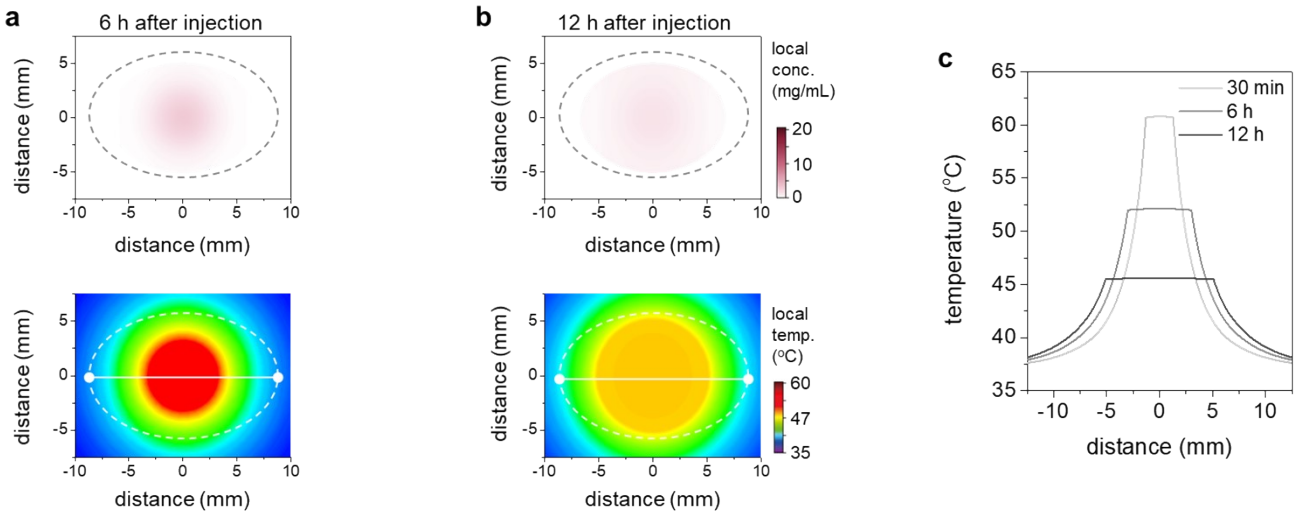

Figure S10. Mass transfer and heat transfer simulation for single-point PSD-SPNP injection. (a,b) Concentration distribution of PSD-SPNP (top) and temperature distribution (bottom) at the tumor after 6 h (a) and 12 h (b). (c) Temperature profile across the tumor (white horizontal lines at heat maps) depending on the diffusion period (30 min, 6 h, and 12 h) of PSD-SPNP. Tumor volume, 0.3 mL, initial nanofluid concentration, 20 mg/mL, nanofluid concentration at tumor, 5 mg/mL$_{tumor}$.

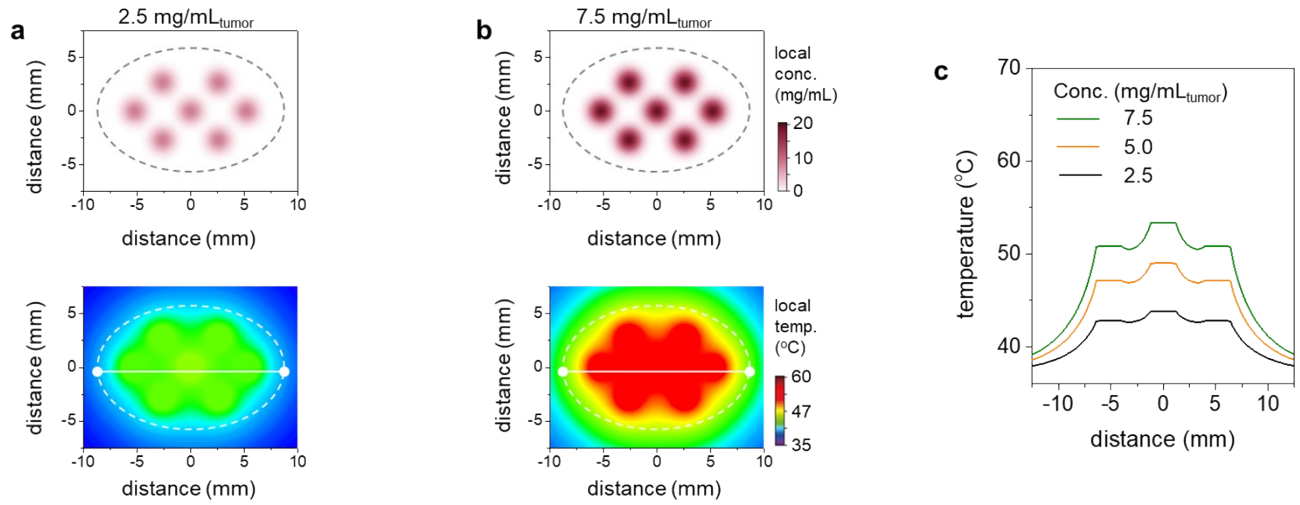

Figure S11. Mass transfer and heat transfer simulation for 7-point PSD-SPNP injection. (a,b) Concentration distribution of PSD-SPNP (top) and temperature distribution (bottom) at the tumor after 30 min with 2.5 mg/mL$_{tumor}$ (a) and 7.5 mg/mL$_{tumor}$ (b) of final mean PSD-SPNP concentration. (c) Temperature profile across the tumor (white horizontal lines at heat maps) depending on the final mean PSD-SPNP concentration of 2.5, 5.0, and 7.5 mg/mL$_{tumor}$. Tumor volume, 0.3 mL, initial nanofluid concentration, 20 mg/mL.

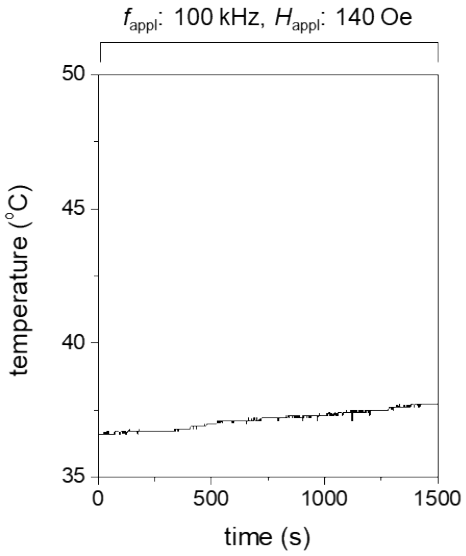

Figure S12. Temperature profile of P-SPNP injected tumor during the MNFH (f_{appl}: 100 kHz, H_{appl}: 140 Oe). Nanofluid concentration at the center of tumor is 5 mg/mL$_{tumor}$.

Supporting Table

d_{MNP} (D_h) (nm)	T_B (K)	K_u (J/m^3)	τ_N (s)	τ_B (s)	τ_{eff} (s)
13 (15)	50	1.19×10^4	6.6×10^{-8}	9.0×10^{-7}	6.2×10^{-8}
25 (30)	280	1.21×10^4	1.6×10	5.8×10^{-6}	5.8×10^{-6}

Table S1: The measured and calculated values of blocking temperature (T_B), K_u, τ_N, τ_B, and effective relaxation time constant (τ_{eff}).

d_{NP} (D_h) (nm)	χ_0	$\frac{2\pi f\tau_{eff}}{1+(2\pi f\tau_{eff})^2}$	χ''
13 (15)	29.2	0.016	0.48
25 (30)	204.6	0.211	35.22
30 (35)	300.1	0.126	22.90
35 (40)	389.5	0.098	16.82

Table S2. Calculated out-of-phase susceptibility (χ'').

References

(1) Rosensweig, R. E. Heating Magnetic Fluid with Alternating Magnetic Field. *J. Magn. Magn. Mater.* **2002**, *252*, 370–374.

(2) Tang, Y.; Flesch, R. C. C.; Jin, T. Numerical Analysis of Temperature Field Improvement with Nanoparticles Designed to Achieve Critical Power Dissipation in Magnetic Hyperthermia. *J. Appl. Phys.* **2017**, *122* (3). https://doi.org/10.1063/1.4994309.

(3) PENNES, H. H. Analysis of Tissue and Arterial Blood Temperatures in the Resting Human Forearm. *J. Appl. Physiol.* **1948**, *1*, 93–122. https://doi.org/10.5005/jp/books/12678_10.

(4) Tang, Y. dong; Jin, T.; Flesch, R. C. C. Impact of Different Infusion Rates on Mass Diffusion and Treatment Temperature Field during Magnetic Hyperthermia. *Int. J. Heat Mass Transf.* **2018**, *124*, 639–645. https://doi.org/10.1016/j.ijheatmasstransfer.2018.03.096.

(5) Suleman, M.; Riaz, S. In Silico Study of Hyperthermia Treatment of Liver Cancer Using Core-Shell CoFe2O4@MnFe2O4 Magnetic Nanoparticles. *J. Magn. Magn. Mater.* **2020**, *498* (November 2019). https://doi.org/10.1016/j.jmmm.2019.166143.

(6) Tang, Y. dong; Jin, T.; Flesch, R. C. C. Effect of Mass Transfer and Diffusion of Nanofluid on the Thermal Ablation of Malignant Cells during Magnetic Hyperthermia. *Appl. Math. Model.* **2020**, *83*, 122–135. https://doi.org/10.1016/j.apm.2020.02.010.

(7) Pavel, M.; Gradinariu, G.; Stancu, A. Study of the Optimum Dose of Ferromagnetic Nanoparticles Suitable for Cancer Therapy Using MFH. *IEEE Trans. Magn.* **2008**, *44* (11 PART 2), 3205–3208. https://doi.org/10.1109/TMAG.2008.2001661.